Senior Thesis

Rachel Y. Ha

University of Washington

School of Oceanography

Seattle WA

rachelh9@uw.edu

5 June, 2026

Running Title: Effects of Stratification on the Depth, Intensity and Community Composition of Deep Chlorophyll Maxima in the Western Tropical Pacific

Abstract

The Northern Mariana Islands are located within the West Pacific Warm Pool, a region characterised by year-round warm sea surface temperatures, low salinity, and strong vertical stratification. This stratification limits upward nutrient flux, resulting in oligotrophic surface waters and low satellite-observed chlorophyll concentrations. Satellite observations are limited to the surface layers and often fail to detect the subsurface Deep Chlorophyll Maximum (DCM). The Mariana Volcanic Arc hosts over 60 seamounts, creating variable bathymetry that locally weakens stratification through enhanced mixing, which increases nutrient supply and affects the DCM structure. Using data collected aboard R/V *Thomas G. Thompson* Cruise TN-450, we investigated whether decreasing stratification intensity at seamounts was associated with (1) shallower DCM depth, (2) increased chlorophyll concentration, and (3) a shift in plankton community composition towards a higher trophic level. CTD fluorescence was calibrated against processed chlorophyll water samples, resulting in a moderate calibration R^2 (0.552) that raises uncertainty for calculating DCM metrics. Correlations between stratification and DCM depth, thickness, and intensity were weak and statistically insignificant ($p > 0.05$), suggesting submesoscale variability and episodic mixing had more influence than stratification. Dominance of *Radiolaria* was observed across all stations at DCM. The minimal difference offshore and at seamounts indicates that community structure is more strongly influenced by the Island Mass Effect than local stratification. These results indicate that stratification alone does not explain DCM metrics in this region. Future studies should incorporate nutrient, PAR, and temperature data to evaluate the primary driver of DCM characteristics.

Plain Language Summary

The Northern Mariana Islands are located within the West Pacific Warm Pool, where density differences between warm, fresh surface water and cold, salty deep waters create strong barrier layers within the water column. The barrier, also known as stratification, limits nutrient supply to surface waters, thereby limiting phytoplankton growth and resulting in low surface chlorophyll concentrations. Satellites can only capture the surface chlorophyll concentration and often miss the Deep Chlorophyll Maximum (DCM), subsurface peaks in chlorophyll concentrations. As the region is affected by underwater seamounts, they may increase mixing and supply more nutrients. This study investigates how stratification intensity affects the depth, thickness, chlorophyll concentration, and phytoplankton communities in the DCM of seamount regions compared with nearby open-ocean waters. We predicted that weaker stratification at seamounts would lead to shallower and stronger DCMs, as well as shifts in planktonic taxonomic to secondary producers/consumers. We found an expected significant correlation between CTD fluorescence and sampled chlorophyll concentration. However, no clear relationship was found between how strongly water was layered and the depth or intensity of the chlorophyll layer, and other small-scale wind-driven mixing patterns may be influencing the DCM structure in the region instead. All stations were mostly dominated by secondary producers, *Radiolaria*, suggesting the Island Mass Effect determines the plankton distribution more. Future steps should include nutrient, light and temperature data to obtain a full picture of how DCM metrics are affected by these parameters.

Introduction

Ocean stratification, or density stratification, refers to the layering between two water bodies of different densities, as determined by temperature, salinity and pressure. Typically, a stable stratified water column has less dense, warmer, fresher water sitting on top of denser, usually colder and saltier, water, creating a density gradient with depth (Gill, 1982; Cushman-Roisin & Beckers, 2011; Cheng et al., 2025). Stratification intensity is quantified by the change in density over a depth range at the pycnocline, where density peaks (*See Methods*). Important features include the mixed layer depth

(MLD), which marks the boundary below where mixing is suppressed and determines the upward exchange of nutrients, heat, carbon, and oxygen from bottom waters (Lévy et al., 2001).

The Northern Mariana Islands (CNMI) are located in a tropical region (15° N) within the West Pacific Warm Pool (WPWP), which is characterised by abnormally warm sea surface temperatures (SST) (> 28°C) and low sea surface salinity (SSS) (< 35 PSU) relative to surrounding waters (Donguy, 1987; Levitus, 1983). While SST and SSS in the WPWP vary only slightly across seasons (within 2°C and 1 psu, respectively) (Zweng et al., 2013; Hollstein et al., 2020), a small change in salinity can have a large regional influence in the Western Pacific, affecting stratification intensity (Capotondi et al., 2012). The intense stratification at the WPWP generally prevents upward nutrient supply from bottom waters, resulting in shallower MLD and nutrient-depleted oligotrophic surface waters.

The exceptions are the waters around the Mariana Volcanic Arc, where seamounts typically weaken stratification due to shallower depths and potentially increase nutrient upwelling. Seamounts are underwater landforms that rise 1000m above the seafloor but don't breach the surface ocean (Staudigel et al., 2010; Yesson et al., 2011; Ma et al., 2021). Seamounts include active, dormant, and extinct submarine volcanoes formed by tectonic activity and are thus typically adjacent to subduction zones, mid-ocean ridges or hotspots (Staudigel et al., 2010). The Mariana Volcanic Arc has at least 60 submarine volcanoes along its 1200 km axis, so it would naturally affect bottom-ocean dynamics due to its bathymetry. In particular, ocean currents are diverted and form topographic Rossby waves (TRWs) as they cross a seamount with drastically reduced depth, in accordance with conservation of shallow water potential vorticity (PV = $(\zeta + f)/H$ = (relative vorticity + Coriolis parameter)/ water depth) (Solomon, 1978 Equation 5). These currents can further generate lee waves, a type of internal gravity wave that forms on the lee side (downstream) of seamounts. As lee waves become unstable and break, they create turbulence and secondary waves help transport water masses upward (Jiang et al., 2021). These hydrological phenomena caused by seamounts could thus affect stratification and nutrient enrichment by increasing vertical mixing through upwelling, otherwise known as "the Seamount Effect". Exceptions such as the M2 seamount showed a weaker influence on stratification in the absence of upwelling along the seamount slope (Ma et al., 2023).

Due to the high SST and the oligotrophic nature of tropical waters, the CNMI has low surface [chl-a] as measured by satellite. However, satellite-derived [chl-a] is limited to the first optical depth (Gordon & McCluney, 1975) and cannot detect the existence of the Deep Chlorophyll Maxima (DCM).

DCM is visualised as a single (or sometimes multiple), intense peak in [chl-a] in a depth profile, often between the nutrient-poor MLD and the euphotic zone (Estrada et al., 1993). DCMs generally develop under stratified conditions, and when salinity strengthens the density gradient below the thermocline, a barrier layer can form beneath the MLD, limiting thermal and nutrient mixing between the mixed layer and the underlying thermocline waters (Bosc et al., 2009). In oligotrophic zones, phytoplankton tends to grow in deeper waters where the nutricline and the photic zone intersect. While both light and nutrient availability are important for phytoplankton productivity, we can assume the photic zone depth is constant between 0 and 200m as the CNMI is located within the tropics (Honjo & Okada, 1974). According to Wei et al. (2022), size-fractionated [chl-a] (pico-, nano-, microphytoplankton) were 2 to 4 times higher near the subsurface 100 m than in the surface layer. Understanding the DCM is important because it affects the region's primary productivity (PP), the rate at which phytoplankton convert inorganic carbon (CO_2) into organic matter, primarily through photosynthesis (Falkowski & Raven, 2013). Thus, this highlights the need for in situ observations to study the DCM and its associated phytoplankton communities (Cornec et al., 2021).

Stratification can also affect plankton distribution at the DCM. As mentioned, in oligotrophic zones, more intense stratification could limit upward nutrient transport and push the DCM deeper, closer to the base of the euphotic zone. Changes in light and nutrients do not directly affect zooplankton, but they impact phytoplankton growth, which limits zooplankton grazing. While the Island Mass Effect may also increase nutrient availability through upwelling along the coast, we expect stratification to outweigh this effect at stations farther offshore (De Falco et al., 2022). Thus, it is expected that a higher proportion of zooplankton is found in the DCM in weaker stratified regions (around seamounts), as light and nutrient availability for phytoplankton growth increases and fuels zooplankton growth.

This study assesses how stratification intensity affects the occurrence of DCM by comparing regions near seamounts and open-ocean areas near the CNMI. Since temperature and salinity in the WPWP are relatively constant year-round, the stratification intensity is assumed to be consistent in the open ocean with little variation, as are the DCM depth and intensity. However, seamounts can change stratification intensity. Shallower depths lead to weaker stratification, so a lower buoyancy frequency is observed at seamounts. It is hypothesised that at seamounts, particularly at the summit where the water depth is the shallowest and thus weaker stratification, there is (1) a shallower but (2) more intense DCM, and (3) a shift in plankton composition to a higher trophic level. The shallower water depths at seamounts increase the formation of TRWs and lee waves, which promote upwelling and thus increase mixing and nutrient supply from bottom waters. This would result in weaker stratification and a deeper MLD than in open-water regions. Thus, the expected result is that stratification intensity is positively correlated with DCM depth and negatively correlated with DCM intensity, and zooplankton dominance at DCM will be observed.

Methods

Data collection

Data collection was done in situ on R/V *Thomas G. Thompson* (Cruise TN-450) around the Northern Mariana Islands (13.63-15.68°N, 144.41-148.54°E) from March 22-30, 2026. Out of a total of 68 stations, CTD casts were done at 27 stations, chlorophyll samples were collected at 15 stations, and phytoplankton samples were collected at 8 stations. Stations were classified into seamount or other stations, using the descriptions shown in *Appendix Table A1*.

The CTD onboard is a Sea-Bird SBE 911plus, measuring standard variables such as conductivity, temperature for density calculations, and depth. 24 10-L Niskin bottles and a WET Labs ECO-AFL/FL fluorometer mounted on the CTD rosette were used to collect chlorophyll samples and fluorescence values (Seabird Scientific). Exact target depths for firing Niskin bottles were determined after the CTD downcast, with at least two main target depths at the surface (15m) and at the DCM (usually between 100 and 200m, as observed in fluorescence depth-profile peaks), and up to 10 depths in each cast. Two bottles were fired at each target depth for replicate samples. Water samples are then collected from Niskin bottles in a 1 L opaque amber HDPE bottle to prevent chlorophyll degradation from light (Thermo Scientific Nalgene).

A phytoplankton net of 0.25-m diameter, 20-µm mesh size on the ship's A-frame was used for samples at DCM depth, which was determined by visualising the fluorescence peak on the CTD downcast for each station. The net was open and deployed vertically, upon hitting the target depth, it is closed and immediately retrieved at 30 m min^{-1}. Phytoplankton samples are collected in glass jars and stored in the refrigerator if not analysed immediately.

Lab analyses

Processing of chlorophyll a samples followed the Standard Operating Procedure of Strickland & Parsons (1972). The 1L seawater sample was subsampled into two and filtered through 0.7µm glass-fibre filters (GF/F) on a filtration rack under vacuum, resulting in a total of 136 chlorophyll samples. Chlorophyll was extracted from the filters using the acetone method for 24 hours at -20°C, and the fluorescence of each sample was measured on a TD-700 fluorometer (Turner Designs). During chlorophyll processing, we realised that some stations (Stations 42, 43, 44, 45, 47, 47b, and 48) had used faulty filters, in which fibres dissolved into the acetone chlorophyll solution, potentially skewing 78 processed chlorophyll values.

The Discover Echo Rebel microscope was used for phytoplankton microscopy. Observations were made by switching among 4X, 10X, and 20X objectives to improve visual clarity. 1 mL of each phytoplankton sample was pipetted onto a Palmer-Maloney slide for counting plankton taxa groups. There are five main taxonomic groups we focused on counting: *Bacilliariophyta*, *Ciliophora*, *Dinoflagellata*, *Haptophyta*, and *Radiolaria*. Taxa identification was cross-checked by referencing a plankton annotation guide with descriptive features and pictures listed for each taxon, provided by the OCEAN 443/444/445 teaching team. Counts were also further cross-examined by two observers and compared to ensure count accuracy (*Appendix Figure A4*). Most microscopy work was done within 48 hours to reduce clustering of dead organic matter in the phytoplankton sample.

Data cleaning and processing

Preliminary processing of CTD data was done onboard, and using code provided by OCEAN 445 students, Chris Moon and Lydia Kelley, the standard .cnv files were converted to .csv files with corresponding metadata files for each station, with column names also abbreviated to make subsetting easier. Post-cruise cleaning and data analyses were done in a Jupyter Notebook. Correlation analyses were done using a simple linear regression model.

Of the 136 data points collected from the CTD casts, 10 values with negative bottle [chl-a], 78 values from faulty filters (*See Lab Analyses*), 6 values corresponding to negative CTD fluorescence, and 10 values for depths below 300m were removed during data post-processing. The final [chl-a] bottle dataset contained 32 data points. While negative fluorescence values do occur when CTD fluorescence readings fluctuate near zero depth, we removed them because negative values in linear regression would shift the slope and intercept, potentially skewing the chlorophyll calibration curve. Depths from 300m below were removed as no photosynthetic light can penetrate through, but depths beyond the predicted DCM range (100-160m) were still included to roughly account for the euphotic zone depth.

Quantifying stratification intensity and DCM characteristics

The stratification intensity is determined by the buoyancy frequency (N^2), also known as the Brunt-Väisälä frequency. If N^2 is closer to 0, it indicates an unstable, weakly stratified layer, corresponding to strong mixing in seamount regions. N^2 values at DCM for each station were individually computed via TEOS-10 Gibbs SeaWater toolbox (gsw.Nsquared) using Absolute Salinity (S_A), Conservative Temperature (CT) and pressure (McDougall and Barker, 2011). This calculation is equivalent to Millard et al's buoyancy frequency equation (*Equation 1*).

$$N^2 = \frac{g}{\rho} \times \frac{\Delta\rho}{\Delta z}$$

Equation 1: Buoyancy frequency (N^2) as proxy for stratification intensity, where g is the gravitational constant, ρ is water density, $\Delta\rho$ is the change in density, and Δz is the change in water depth (Millard et al., 1990, Equation 6).

DCM intensity is defined as the total [chl-a] within the DCM range, calculated from depth-integrated [chl-a] using Equation 2. The depths for integration (z) are defined using Full Width Half Maximum (FWHM) at max [chl-a], in which the upper DCM range (z_{upper}) is defined as depth at 0.5 × max [chl-a] above peak [chl-a], and the lower range (z_{lower}) is defined as depth at 0.5 × max [chl-a] below peak [chl-a]. The resulting depth range is defined as our DCM thickness. We used FWHM instead of the more commonly used Gaussian distribution, which uses μ as the DCM peak and σ as edge constraints (Uitz et al., 2006), because it is computationally easier and better suited to asymmetric distributions. It can account for different thicknesses from the DCM peak to the upper or lower edge. Before computing DCM intensity, we first bin the calibrated CTD cast to 1m to minimise noise and spikes. The upper 30m is ignored to avoid daytime non-photochemical quenching at the surface. Any nan values are also ignored when identifying DCM thickness using FWHM. We then locate the DCM using the maximum [chl-a] and its corresponding depth as the DCM depth. However, a limitation of depth-integrated [chl-a] is that it cannot reflect a bimodal DCM structure.

$$Chl_{int} = \int_{z_{lower}}^{z_{upper}} Cz\,(dz)$$

Equation 2: Depth-integrated [chl-a] as proxy for DCM intensity (Morel & Berthon, 1989). C is the [chl-a] at z depth, z_{upper} is the upper integration depth range defined as depth at half [chl-a] maximum above peak, z_{lower} is the lower integration depth range defined as half [chl-a] maximum below peak.

Results

Calibration of CTD Fluorescence to Chlorophyll Concentration

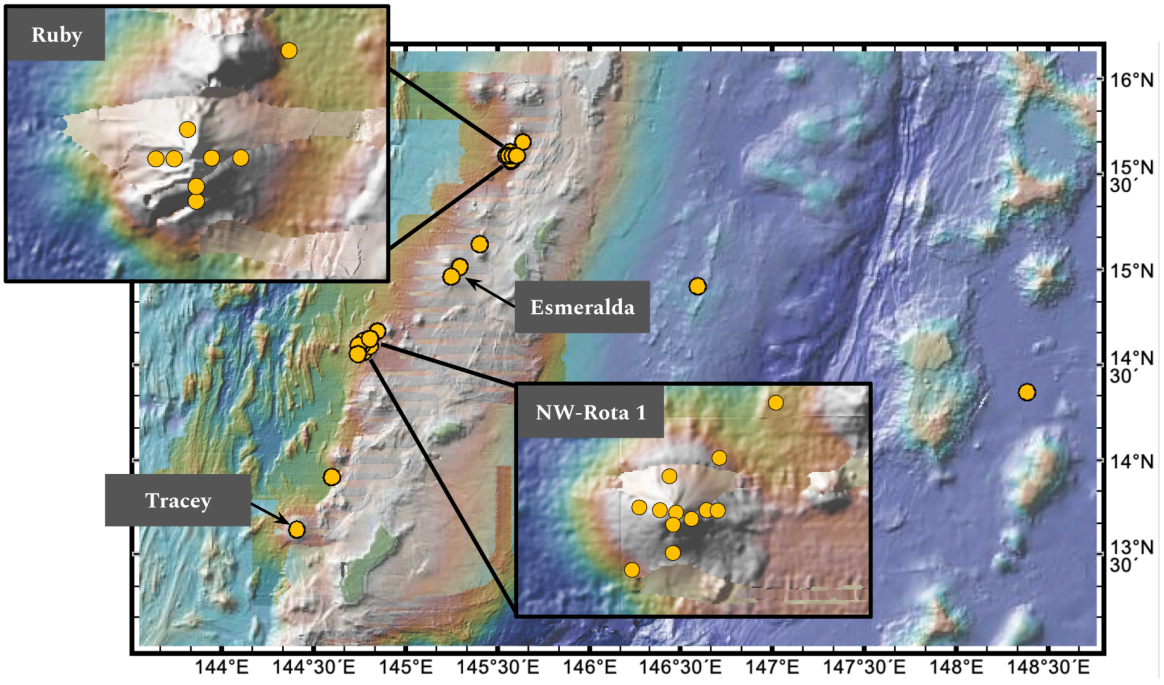

Figure 1: Map of stations on R/V *Thomas G. Thompson* TN-450 cruise around the Northern Mariana Islands. CTD cast data as indicated by the yellow circle markers (*see Appendix Table A1 for all stations*). Seamount

regions are labelled and zoomed in to display the full transect of CTD casts (Figure made with GeoMapApp (www.geomapapp.org) / CC BY / CC BY (Ryan et al., 2009)).

The TN-450 cruise sampled CTD casts at seamounts and open ocean regions near the CNMI (*Figure 1*). Seamount samples were collected across four seamounts, Ruby, Esmeralda, NW Rota-1 and Tracy, at their respective summits, upstream and downstream environments. Most stations sampled on the west side of CNMI had relatively shallow bathymetry, and only 2 stations east of CNMI had deeper depths at ~3000-4000m.

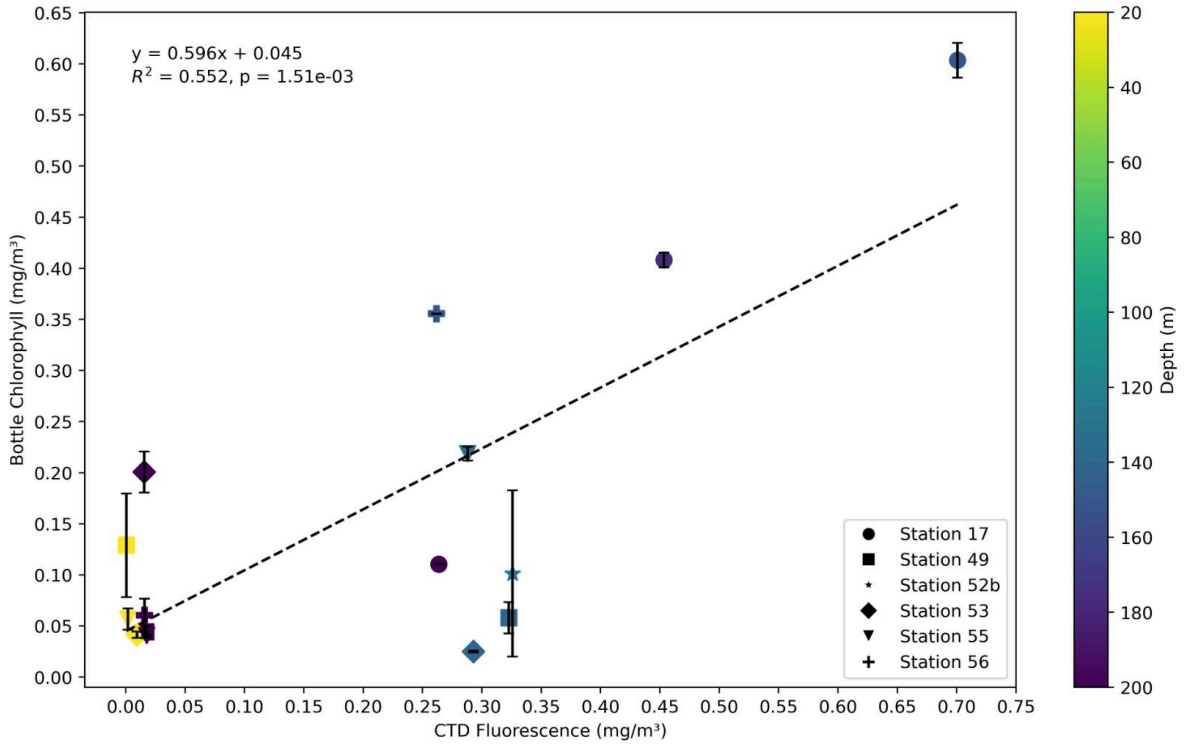

Figure 2: Chlorophyll calibration curve, with a total of 15 data points of mean bottle chlorophyll (mg/m^3) plotted against CTD Fluorescence (mg/m^3). The depth of data points is indicated by colour. Error bars, shown in black, indicate the standard deviation of the mean of bottle chlorophyll values post-cleaning. The linear regression equation between the two variables is given as: y = 0.596x + 0.045. R^2 value is 0.552 and p-value is 1.51×10^{-3}.

A calibration curve is created to correct for the CTD fluorescence values. The chlorophyll calibration curve was based on 15 data points, obtained by averaging [chl-a] at the same depths across stations in the 32 cleaned data points (*See Methods*). Station 17 had 4 [chl-a] values at 150m, which were averaged into one, resulting in an odd number of data points. CTD fluorescence on the x-axis and [chl-a] is plotted on the y-axis. The standard deviation of the average bottle chlorophyll concentration, shown as the black error bars, is relatively small, except for the data point averaged across 4 values, which has the largest standard deviation of 0.7008. Data points were also coloured by depth to examine if values of similar depths cluster together. Most values are clustered with depth, except in the 120-160m depth range. The regression equation (y = 0.596x + 0.045) was used for correcting CTD fluorescence to [chl-a]. The computed value for [chl-a] is calculated by multiplying the slope (0.596) by the fluorescence values (x) and adding the y-intercept offset value (0.045). The positive slope indicates a slightly positive relationship between the two variables. R^2 value is 0.552, and p-value is 1.51×10^{-3} (<0.05), showing a relatively moderate but statistically significant correlation.

Corrected [chl-a] depth profiles with DCM metrics

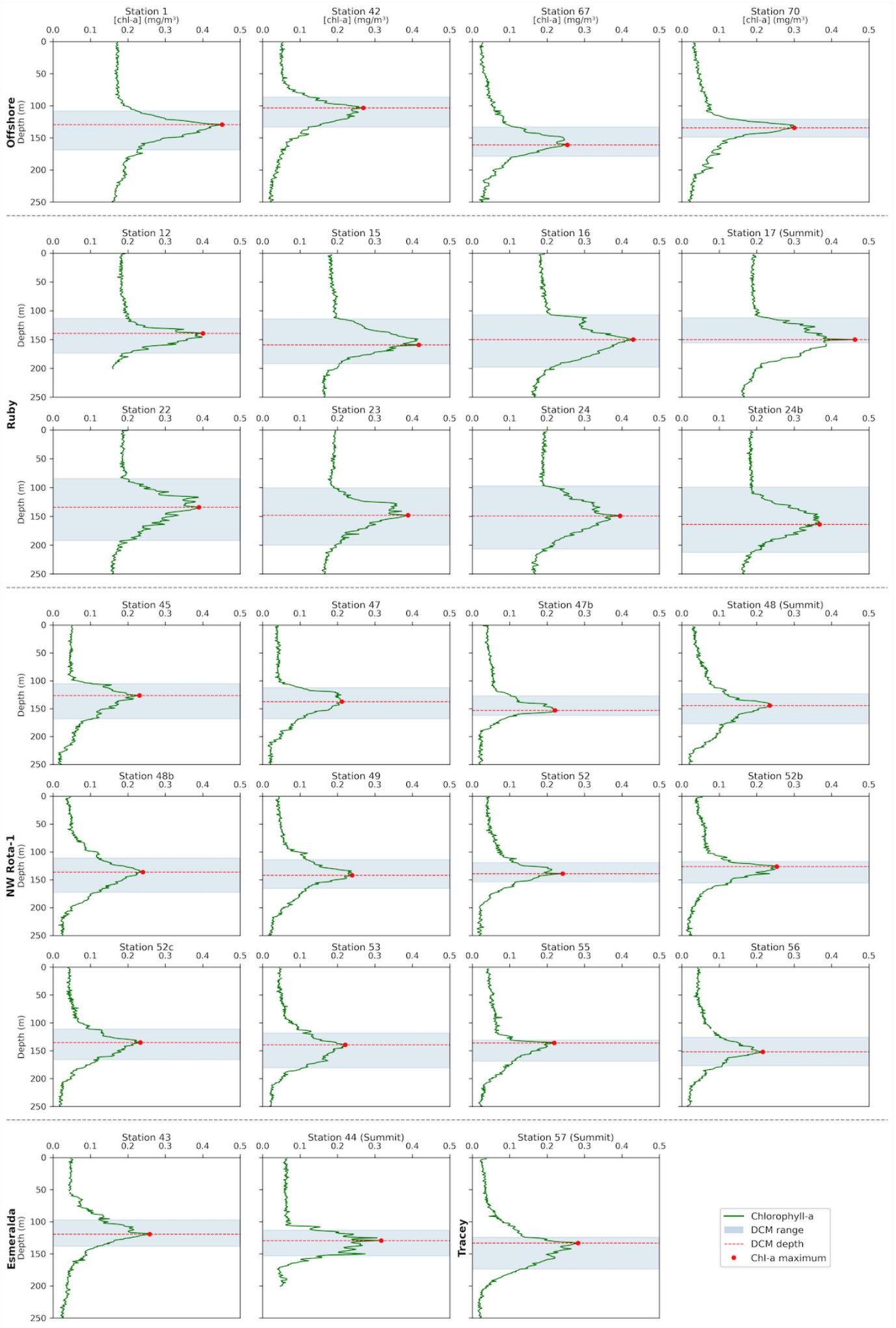
Offshore
Ruby
NW Rota-1
Esmeralda
Tracey
Station 1
Station 42
Station 67
Station 70
Station 12
Station 15
Station 16
Station 17 (Summit)
Station 22
Station 23
Station 24
Station 24b
Station 45
Station 47
Station 47b
Station 48 (Summit)
Station 48b
Station 49
Station 52
Station 52b
Station 52c
Station 53
Station 55
Station 56
Station 43
Station 44 (Summit)
Station 57 (Summit)
[chl-a] (mg/m³)
Depth (m)
Chlorophyll-a
DCM range
DCM depth
Chl-a maximum

Figure 3: Post-calibration [chl-a] depth profiles at 27 stations, divided into offshore, Ruby, NW-Rota, Emeralda and Tracey stations. Black dashed lines indicate DCM upper and lower boundaries, defined as the DCM thickness. The red dot shows the [chl-a] peak, which represents the DCM. The pink dashed line indicates the DCM depth.

Calibrated [chl-a] profiles showed a distinctive peak at depths ranging from 100 to 160m across all stations, with a mean DCM depth of 139.6m and a standard deviation of 13.3m. Potential bimodal distributions were seen at Ruby, Esmeralda and Tracey stations, with one additional peak aside from the max chl marker identified on *Figure 3*. The largest DCM ranges were found at stations around the Ruby seamount (*Stations 12, 15-17, 22-24, 24b*), averaging around 87m thick, whereas the mean DCM thickness was 59.7m across 27 stations. Ruby and Esmerelda summit had thinner DCM and the highest [chl-a] compared to their surrounding stations, at 0.463mg/m^3 and 0.316mg/m^3, respectively. Stations at each seamount had a similar DCM depth. The DCM depth at Ruby peaked between 140 and 160m, while Esmerelda had a shallower DCM depth at around 120-130m. However, the narrowest DCM thickness was found at Station 70, an offshore station west of the Mariana Trench, with a thickness of 27.8m.

Visualising DCM depth, thickness and intensity VS stratification intensity across stations

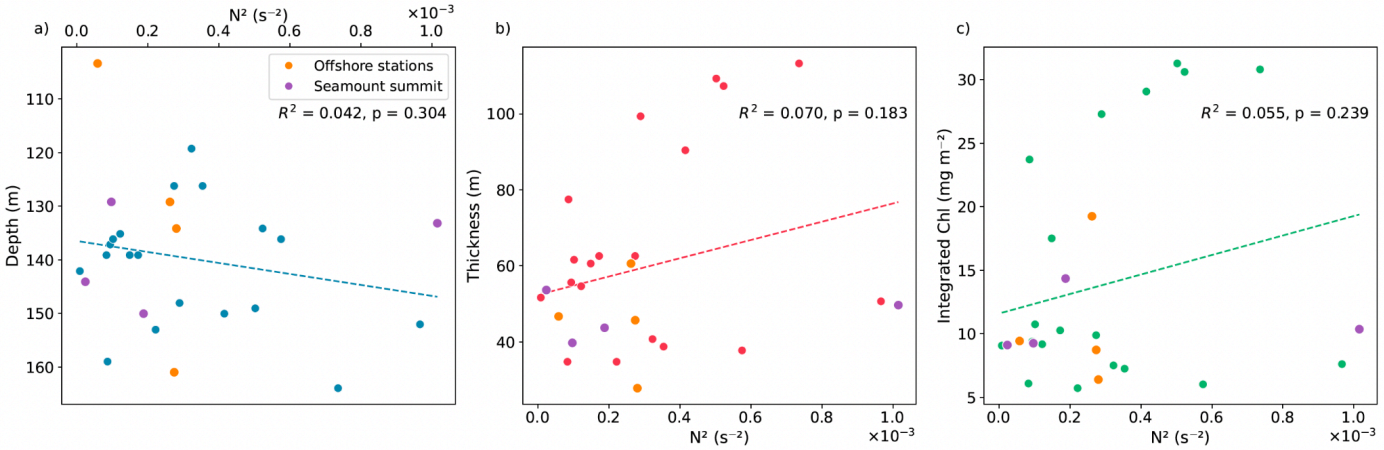

Figure 4: (a) Buoyancy frequency (N^2) vs DCM depth across 27 stations (R^2 = 0.042, p = 0.304) labelled with blue data points. (b) N^2 vs DCM thickness (R^2 = 0.070, p = 0.183) labelled in red data points. (c) N^2 vs DCM depth-integrated [chl-a] (R^2 = 0.055, p = 0.239) labelled in green data points. Purple markers indicate seamount summit stations, while orange data points indicate offshore stations.

To test our hypotheses about the relationship between stratification intensity and DCM metrics, correlation analyses were conducted for each pair of metrics and N^2. All three metrics – DCM depth, DCM thickness and DCM-integrated [chl-a] – showed a weak but positive correlation with stratification, with DCM depth having the weakest correlation (R^2 = 0.042) and DCM thickness having relatively the strongest (R^2 = 0.070) (*Figure 4a,b,c*). None of the three DCM metrics showed a statistically significant relationship with N^2 at the DCM depth ($p > 0.05$). Values of DCM metrics scatter across low N^2 values, stations with the weakest stratification have the widest ranges in DCM depth, thickness, and intensity. While offshore stations had a similar range in N^2, they had a varying range in DCM depths ranging from 103m to 160m. Whereas for seamount summit stations, they had a similar range for each DCM metric, but an outlier with an abnormally higher N^2 value of 1.0×10^{-3} s^{-1} compared to the 0.1×10^{-3} s^{-1} average of the other 3 stations.

Plankton distribution at DCM

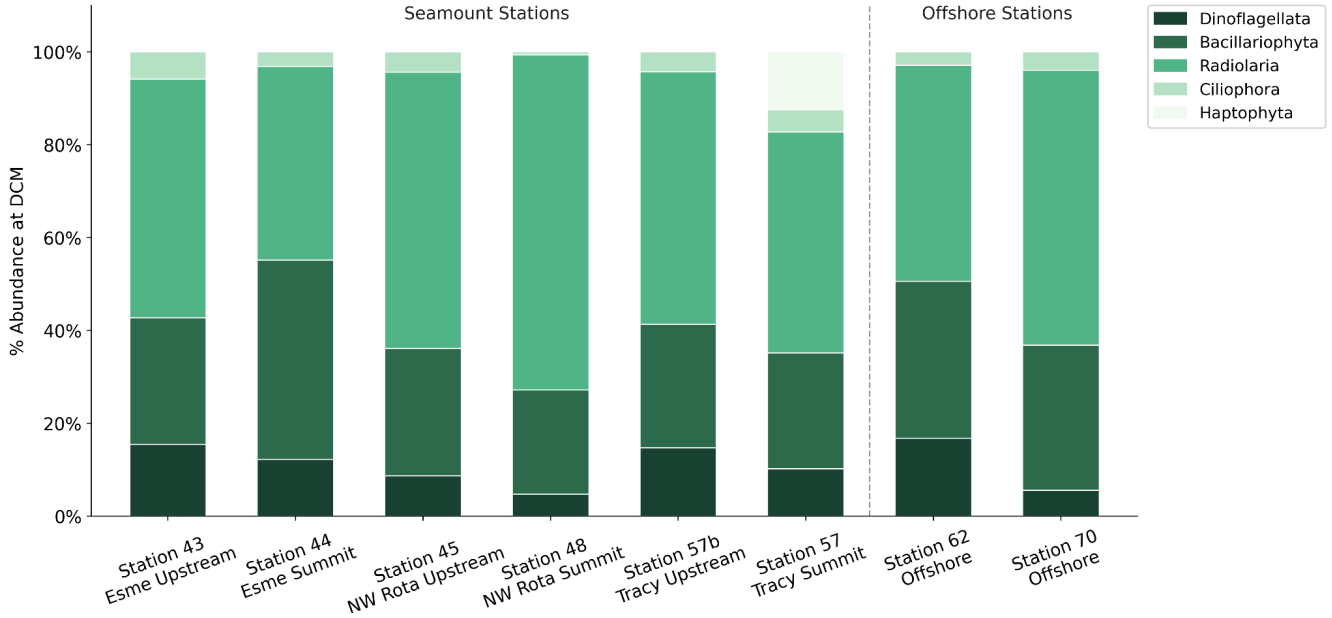

Figure 5: Percentage abundance of plankton taxa groups in samples at the DCM (*See Appendix Table A5 Observer A log*). A total of 8 stations were separated into seamount and offshore stations. Five taxonomic groups were identified: *Bacilliariophyta*, *Ciliophora*, *Dinoflagellata*, *Haptophyta*, and *Radiolaria*.

The percentage distribution of each plankton group identified within the DCM shows little difference between seamount and offshore stations (*Figure 5*). *Radiolaria* dominance was seen across all stations, with the highest percent (72.2%) observed at Station 48 compared to the 41-59% range for other stations. Offshore stations had slightly lower average *Radiolaria* percentage abundance (52.85%) than seamount stations (54.48%), but the lowest (41.7%) was observed at the Esmeralda Summit Station 44. *Bacillariophyta* percentage abundance was 1.2% more than *Radiolaria* at Station 44, but closely followed as the second most abundant group for other stations. *Ciliophora* and *Haptophyta* are nearly absent (0.6-5.9% and 12.5% at one station, respectively), while *Dinoflagellata* are consistently the third largest across all stations.

Discussion

Chlorophyll calibration

CTD fluorescence is usually used as a proxy for [chl-a], but raw fluorescence values may under- or overestimate [chl-a] due to photoacclimation effects, depending on light availability. From *Figure 2*, our calibration curve had an R^2 of 0.552 ($p < 0.05$), indicating that the remaining 45% of the variance in fluorescence was not explained [chl-a]. This raises concerns about the confidence of our [chl-a] depth profiles post-calibration, as the moderate R^2 value could potentially skew the accuracy of predicting DCM metrics used for correlation plots against stratification. While it is important to use high-quality data to ensure the calibration curve's accuracy (Marrec et al., 2025), we minimised inaccuracies by cleaning the data (*See Methods*) and testing different linear regression methods to identify the best R^2 and p-value. A fixed y-intercept is usually applied for the chlorophyll calibration equation, as the general assumption of zero fluorescence equates to zero [chl-a]. However, in our case, we used an equation with a free y-intercept rather than a fixed intercept because the CTD data contain negative fluorescence values, which make [chl-a] uninterpretable when corrected using a multiplication factor from the fixed-intercept equation (*see Appendix Figure A2)*. We also tested to account for day-versus-night calibration differences, as chlorophyll fluorescence depends on light. While the R^2 value of the day calibration curve shows a significantly stronger correlation ($R^2 = 0.918$, $p = 4.24 \times 10^{-10}$), the calibration curve for the night was negative, which is conceptually incorrect

since fluorescence scales positively with concentration (*see Appendix Figure A3)*. Thus, all fluorescence values were calibrated using a single calibration equation in *Figure 2* ($y = 0.596x + 0.045$).

Stratification and DCM metrics

Looking at our correlation plots (*Figure 4*), all correlations were weak and positive, which contradicted part of our original hypotheses, though they were insignificant ($p > 0.05$). Our hypotheses were that a decrease in stratification would be associated with (1) a shallower DCM depth (positive correlation) & (2) stronger DCM intensity (negative correlation). While (1) showed the expected positive relationship, (2) was inverted and instead weaker stratification showed weaker DCM intensity. A possible explanation would be that nutrient upwelling is still occurring, but vertical mixing is so strong that it is diluting nutrients while deepening the mixed layer. This pushes the plankton deeper into the water column, limiting both light and nutrients for their growth (Cornec et al., 2021). The [chl-a] profiles (*Figure 3*) show that DCM across stations were found between 100 and 160m depth, which is supported by previous literature (Furuya, 1990). Despite similar DCM depth ranges between stations, the shape and intensity of the DCM varied within each seamount/offshore category. This is expected as each site is assumed to have different stratification patterns. Looking back at *Figure 4,* stations with the weakest stratification have the widest ranges in DCM depth, thickness, and intensity, suggesting that under weakly stratified conditions, other physical or biological drivers may play a more prominent role in structuring the DCM than stratification does. This may include submesoscale variability and episodic mixing events from storms that provide nutrient input into the DCM layer. It has been suggested that there is a strong relationship between new production, phytoplankton subduction & relative vorticity, so increase in [chl-a] may be by strong horizontal mixing of nutrients from submesoscale density and vorticity gradients (Lévy et al., 2001).

However, this study had a few assumptions. We expected the "seamount effect" to have a constant impact on stratification, but from our [chl-a] depth profiles, no obvious differences in [chl-a] between seamounts and offshore stations were seen (*Figure 3*). Seamount summit stations did not exhibit shallower or more intense DCMs than upstream or offshore stations, even though seamount-induced upwelling has been shown to enhance local productivity in some systems (Genin, 2004; Ma et al., 2021). Ma et al.'s (2023) study have shown that the M2 seamount has no effect on stratification, and our study assumes that seamounts cause an increase in stratification throughout the region. Thus, if there were changes in DCM depth and [chl-a], we cannot fully determine if seamounts were the main influence on stratification. The uncertainty can be shown looking at the seamount summit stations (*See purple markers in Figure 4*), they all fall within a similar range in DCM depth, thickness and integrated [chl-a], with the exception of Tracey seamount with the 1.0×10^{-3} s^{-1} N^2 value. The anomaly may be attributed to the hydrothermal and tectonic activity associated with a small cluster of basaltic underwater volcanoes on the southwest side of Tracey, otherwise known as the Alphabet Seamount Volcanic Province (ASVP) (Stern et al., 2012).

Secondly, we did not include parameters such as photosynthetically active radiation (PAR) and nutrients. Light and nutrients are the two main factors for facilitating phytoplankton growth. From our study, the insignificant correlations ($p > 0.05$) between N^2 and DCM metrics indicate that stratification intensity alone does not explain DCM depth, thickness, or intensity across stations, and the nutricline depth may play a role instead. We also used a baseline of 300m depth as our euphotic zone limit, which is not fully representative of the actual euphotic zone where PAR is 1% of the surface. Therefore, both nutrient and PAR data should be incorporated for further validation for both method and results.

Lastly, our study is based on data collected from a single time point. While SST is relatively consistent within the West Pacific all year round, studies have shown the WPWP has experienced 0.29°C warming for SST above 28.5°C per 50 years since 1955 (Cravatte et al., 2009). In the long term, thermoclines will shift and have a doubling impact on top of the halocline impact on determining stratification (Ma et al., 2021, 2023). So future studies should also account for temperature when observing long-term trends in how global warming can make thermocline a determinant in stratification, which impacts the studied DCM metrics.

Plankton community composition

The taxonomic composition at the DCM was dominated by *Radiolaria* and *Bacillariophyta* across all stations, with minimal differences between seamount and offshore sites. While the dominance of Radiolaria across stations is expected, as they are heterotrophic protists associated with oligotrophic, stratified waters (Llopis Monferrer et al., 2025), there was no significant shift in zooplankton dominance from offshore to seamount regions. *Radiolaria* percentage abundance was similar, with only a 2% difference between seamount and offshore stations *(Figure 5*). The persistent dominance of *Radiolaria,* even at offshore stations, suggests that our hypothesis (3) may require an alternative explanation. Rather than being driven by stratification, plankton community composition may be more influenced by the Island Mass Effect (IME). IME also supplies enhanced nutrient input to the euphotic layer through upwelling, though primarily due to physical processes associated with proximity to islands (De Falco et al., 2022). However, note that there may be incorrectly identified haptophyta, as they cannot be seen with our microscope setup at a maximum magnification of 20X. Thus, a more accurate plankton count is needed, specifically for phytoplankton taxa, to capture the big-picture shift in community composition from phytoplankton to zooplankton.

Conclusions

In this study, we addressed the importance of calibrating CTD fluorescence and, most importantly, of identifying a relationship between stratification intensity and DCM characteristics, including DCM depth, thickness, and intensity.

Correlations between stratification intensity and DCM depth, thickness, and integrated chlorophyll were weak and statistically insignificant across all stations, suggesting that stratification alone is insufficient to explain DCM variability in this region, and that additional drivers such as the nutricline depth, PAR, and episodic mixing events likely play important roles. Observed plankton community composition also aligned with previous findings, in which Radiolaria was favoured in oligotrophic environments, suggesting that the region's plankton composition is influenced by the IME more than stratification. Overall, stratification alone does not determine DCM metrics and composition.

This study focuses on the effects of stratification on DCM characteristics in oligotrophic regions only and is not indicative of global patterns in other subtropical regions or in seasonally stratified oceans. We assumed a constant negative effect of seamounts on stratification, but results showed exceptions like Tracey Seamount with its close proximity to the ASVP, suggesting regional variability of the "seamount effect". Further study may include evaluating submesoscale eddies in oligotrophic regions as a source of nutrient input from upwelling waters and incorporating nutrient, PAR and temperature data to test our alternative hypothesis that these other parameters are the main driver of DCM metrics.

Acknowledgements

I would first like to thank the R/V *Thomas G. Thompson* Cruise TN450 captain and crew for making the cruise operations run smoothly. I would also like to thank my advisor, Dr Francios Ribalet, and other OCEAN 445 instructors for their guidance. Lastly, thanks to all my fellow OCEAN 445 peers for assisting in data collection and processing chlorophyll and phytoplankton samples. This work is funded by the University of Washington School of Oceanography.

Statement of third party and AI use

AI-assisted writing tools, such as Perplexity and Grammarly, were used to summarise reference articles and correct spelling and grammatical errors. Claude AI has been used to troubleshoot and debug code. I have proofread and fact-checked the content changed by AI, and no additional content was generated from AI.

Appendix

Station	Region/ Description	Latitude	Longitude
1	Shake down	13.91128	144.6
12	Upstream Ruby	15.6726	145.6404
15	South Ruby Seamount	15.5721	145.5761
16	South Ruby Seamount	15.582	145.5761
17	Summit of Ruby Seamount	15.62	145.57
22	West of Ruby Seamount	15.6004	145.548
23	West of Ruby	15.6005	145.5607
24	East of Ruby	15.6009	145.5867
24b	East of Ruby	15.601	145.607
42	Coastal Saipan	15.1354	145.4052
43	Upstream Esmerelda	15.0186	145.2976
44	Esmerelda Bank Seamount	14.9667	145.25
45	Upstream NW Rota-1	14.6804	144.8498
47	N of NW Rota-1	14.6291	144.7727
47b	N of NW Rota-1	14.617	144.7726
48	Summit of NW Rota-1	14.601	144.775
48b	S of NW Rota-1	14.5922	144.7728
49	S of NW Rota-1	14.5717	144.7727
52b	E of NW Rota-1	14.6027	144.7979
52	E of NW Rota-1	14.6024	144.8062
52c	W of NW Rota-1	14.6027	144.763
53	W of NW Rota-1	14.6047	144.7475
55	NW of NW Rota-1	14.64046	144.8075
56	SW of NW Rota-1	14.5594	144.74213
57	Tracy	13.633	144.41
67	Offshore Grid	14.3581	148.3857
70	W of trench	14.9151	146.5928

Table A1: Table of 27 stations in which CTD casts were done. Stations are labelled with their respective regions (seamount or offshore). Highlighted rows are seamount summits.

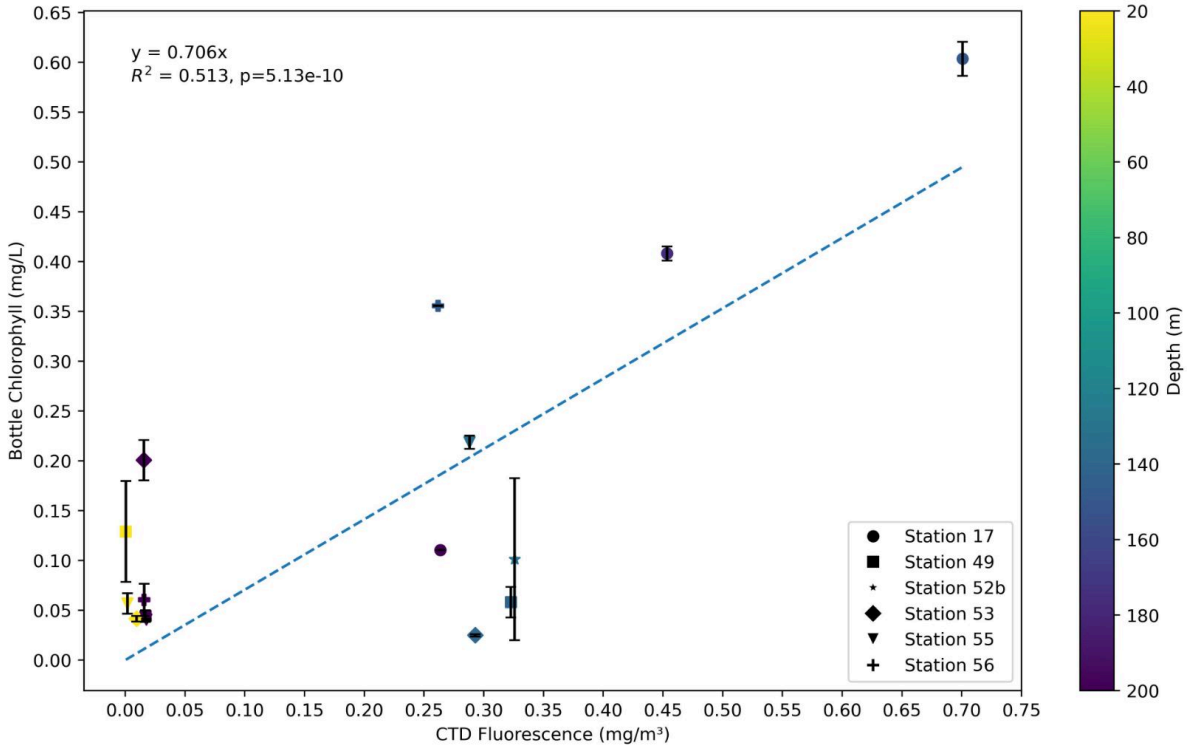

Figure A2: Chlorophyll calibration curve with fixed y-intercept.

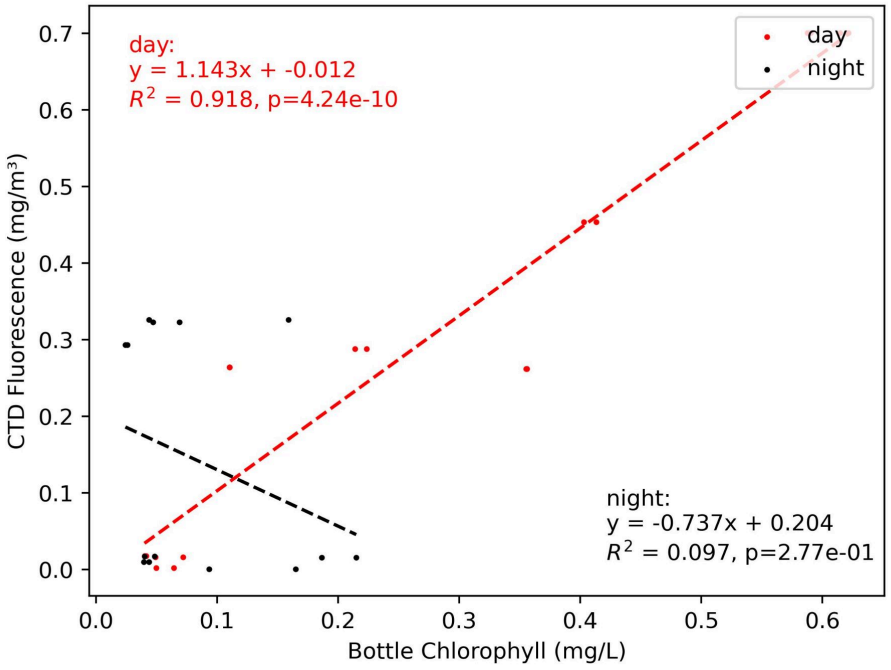

Figure A3: Chlorophyll calibration curve of day vs night with free y-intercept.

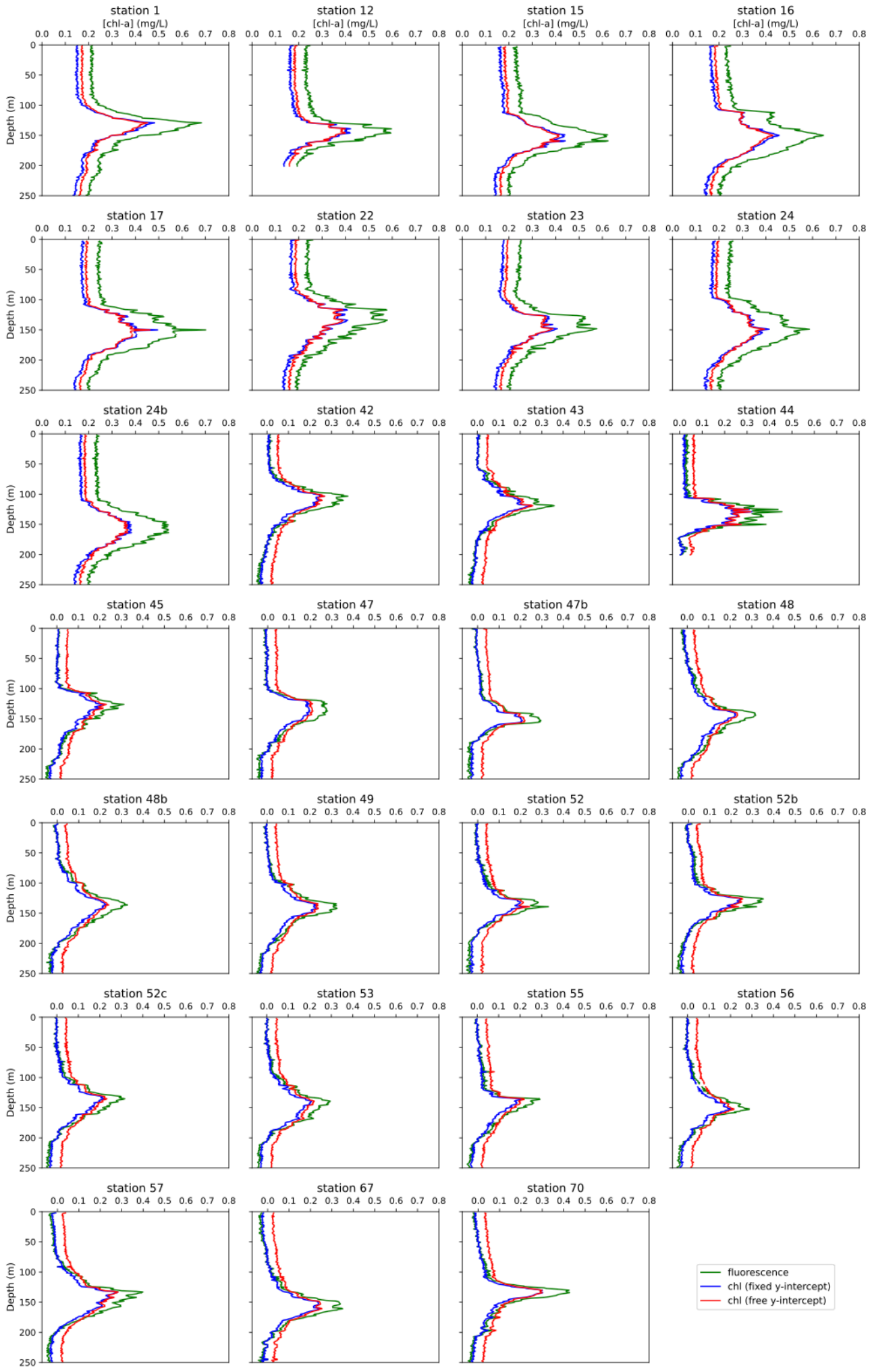
station 1
station 12
station 15
station 16
station 17
station 22
station 23
station 24
station 24b
station 42
station 43
station 44
station 45
station 47
station 47b
station 48
station 48b
station 49
station 52
station 52b
station 52c
station 53
station 55
station 56
station 57
station 67
station 70
[chl-a] (mg/L)
Depth (m)
fluorescence
chl (fixed y-intercept)
chl (free y-intercept)

Figure A4: Chlorophyll depth profiles of 27 stations (pre and post-calibration)

		% Abundance of Major Taxa by Observer					Abundance Rank (1 = Most, 5 = Least)				
Observer	Station	Dino	Bacillario	Radio	Cilio	Hapto	Rank 1	Rank 2	Rank 3	Rank 4	Rank 5
A	43	15.5	27.2	51.4	5.9	0	Radio	Bacillario	Dino	Cilio	Hapto
B	43	18.9	45.9	22.5	11.7	0.9	Bacillario	Radio	Dino	Cilio	Hapto
B-A	*43*	*3.4*	*18.7*	*22.5*	*5.8*	*0.9*					
A	44	12.2	42.9	41.7	3.1	0	Bacillario	Radio	Dino	Cilio	Hapto
B	44	9.3	34.5	27.8	13.4	14.9	Bacillario	Radio	Cilio	Dino	Hapto
B-A	*44*	*-2.9*	*-8.4*	*-13.9*	*10.3*	*14.9*					
A	48	4.7	22.5	72.2	0.6	0	Radio	Bacillario	Dino	Cilio	Hapto
B	48	16.3	48.8	22.1	5.8	7	Bacillario	Radio	Dino	Cilio	Hapto
B-A	*48*	*11.6*	*26.3*	*-50.1*	*5.2*	*7*					
Mean B-A	*43,44,48*	*4*	*12.2*	*-13.8*	*7.1*	*7.6*					

Table A5: Plankton observer log comparison

References

Bosc, C., Delcriox, T., & Maes, C. (2009). Barrier layer variability in the western Pacific warm pool from 2000 to 2007. *Journal of Geophysical Research Oceans, 114*(C6). https://doi.org/10.1029/2008JC005187

Capotondi, A., Alexander, M.A., Bond, N.A., Curchitser, E.N., & Scott, J.D. (2012). Enhanced upper ocean stratification with climate change in the CMIP3 models. *Journal of Geophysical Research: Oceans*, *117*, C4. https://doi.org/10.1029/2011JC007409

Cheng, L., Li, G., Long, S.M., Li, Y., Schuckmann, K.V., Trenberth, K.E., et al. (2025). Ocean stratification in a warming climate. *Nature Reviews Earth & Environment, 6*, 637-655. https://doi.org/10.1038/s43017-025-00715-5

Cornec, M., Claustre, H., Mignot, A., Guidi, L., Lacour, L., Poteau, A., D'Ortenzio, F., Gentili, B., & Schmechtig, C. (2021). Deep Chlorophyll Maxima in the Global Ocean: Occurrences, Drivers and Characteristics. *Global Biogeochemical Cycles*, *35*(4). https://doi.org/10.1029/2020GB006759

Cravatte, S., Delcroix, T., Zhang, D., McPhaden, M., & Leloup, J. (2009). Observed freshening and warming of the western Pacific Warm Pool. *Climate Dynamics, (33)*, 565-589. https://doi-org.offcampus.lib.washington.edu/10.1007/s00382-009-0526-7

Cushman-Roisin, B., and J.-M. Beckers (2011). *Introduction to Geophysical Fluid Dynamics: Physical and Numerical Aspects,* 2nd Edition, 845 pp., Academic Press, Oxford, U. K.

De Falco, C., Desbiolles, F., Bracco, A. & Pasquero, C. (2022). Island Mass Effect: A Review of Oceanic Physical Processes. *Frontiers in Marine Science, 9*. https://doi.org/10.3389/fmars.2022.894860

Donguy, J. (1987). Recent advances in the knowledge of the climatic variations in the tropical Pacific ocean. *Progress in Oceanography, 19*(1), 49-85. https://doi.org/10.1016/0079-6611(87)90003-6

Estrada, M., Marrasé, C., Latasa, M., Berdalet, E., Delgado, M., & Reira, T. (1993). Variability of deep chlorophyll maximum characteristics in the Northwestern Mediterranean. *MarineEcology Progress Series, 92*(3), 289-300. https://doi.org/10.3354/meps092289

Falkowski, P. G., & Raven, J. A. (2013). *Aquatic Photosynthesis*, 2nd edition, 488pp., Princeton University Press, New Jersey.

Furuya, K. (1990). Subsurface chlorophyll maximum in the tropical and subtropical western Pacific Ocean: Vertical profiles of phytoplankton biomass and its relationship with chlorophylla and particulate organic carbon. *Marine Biology, 107*, 529-539. https://doi.org/10.1007/BF01313438

Genin, A. (2004). Bio-physical coupling in the formation of zooplankton and fish aggregations over abrupt topographies. *Journal of Marine Systems, 50*(1-2), 3-20. https://doi.org/10.1016/j.jmarsys.2003.10.008

Gill, A. E. (1982). *Atmosphere–Ocean Dynamics*, 662 pp., Academic Press, New York.

Gordon, H.R., & McCluney, W.R. (1975). Estimation of the Depth of Sunlight Penetration in the Sea for Remote Sensing. *Applied Optics, 14*(2), 413-416. https://doi.org/10.1364/AO.14.000413

Hollstein, M., Mohtadi, M., Kienast, M., Rosenthal, Y., Groeneveld, J., Oppo, D.W., Southon, J. R., & Lückge, A. (2020). The Impact of Astronomical Forcing on Surface and Thermocline Variability Within the Western Pacific Warm Pool Over the Past 160 kyr. *Paleooceanography and Palaeoclimatology, 35*(6). https://doi.org/10.1029/2019PA003832

Honjo, S., & Okada, H. (1974). Community Structure of Coccolithophores in the Photic Layer of the Mid-Pacific. *Micropaleontology, 20*(2), 209-230. https://doi.org/10.2307/1485061

Jiang, X., Dong, C., Ji, Y., Wang, C.S., Shu, Y., Liu, L., & Ji, J. (2021). Influences of Deep-Water Seamounts on the Hydrodynamic Environment in the Northwestern Pacific Ocean. *Journal of Geophysical Research: Oceans, 126*(12), e2021JC017396. https://doi.org/10.1029/2021JC017396

Levitus, S. (1983). Climatological Atlas of the World Ocean. *Eos Transactions American Geophysical Union, 64*(49), 962-963. https://doi.org/10.1029/EO064i049p00962-02

Lévy, M., Klein, P., & Treguier, A. (2001). Impact of sub-mesoscale physics on production and subduction of phytoplankton in an oligotrophic regime. *Journal of Marine Research, 59*(4). https://elischolar.library.yale.edu/journal_of_marine_research/2401

Llopis Monferrer, N., Romac, S., Laget, M., Nakamura, Y., Biard, T., & Sandin, M. M. (2025). Is the Gelatinous Matrix of Nassellaria (Radiolaria) a Strategy for Coping With Oligotrophy?. Environmental microbiology, 27(5), e70098. https://doi.org/10.1111/1462-2920.70098

Ma, J., Song, J., Li, X., Wang, Q., Sun, X., Zhang, W. & Zhong, G. (2021). Seawater stratification vs. plankton for oligotrophic mechanism: A case study of M4 seamount area in the Western Pacific Ocean. *Marine Environmental Research, 169*, 105400. https://doi.org/10.1016/j.marenvres.2021.105400

Ma, J., Li, X., Song, J., Wang, Q., Wen, L., Xu, K., Zhong, G., Dai, J., Xing, J., & Tian, D. (2023). Relationship and stratification of multiple marine ecological indicators: A case study in the M2 seamount area of the Western Pacific Ocean. *Ecological Indicators, 146*, 109804. https://doi.org/10.1016/j.ecolind.2022.109804

Marrec, P., Herbst, A., Beaulieu, S.E. & Menden-Deuer, S. (2025). Hands-on post-calibration of in vivo fluorescence using open access data: A guided journey from fluorescence to phytoplankton biomass. *Oceanography, 38*(2), 73–82, https://doi.org/10.5670/oceanog.2025.314.

McDougall, T.J., & Barker, P.M. (2011). Getting started with TEOS-10 and the Gibbs Seawater (GSW) Oceanographic Toolbox, 28pp., SCOR/IAPSO WG127, ISBN 978-0-646-55621-5.

Morel, A., & Berthon, J.(1989). Surface pigments, algal biomass profiles, and potential production of the euphotic layer: Relationships reinvestigated in view of remote-sensing applications. *Limonology and Oceanography, 34*(8), 1545-1562. https://doi.org/10.4319/lo.1989.34.8.1545

Millard, R.C., Owens, W.B., & Fofonoff, N.P. (1990). On the calculation of the Brunt-Väisäla frequency. *Deep Sea Research Part A. Oceanographic Research Papers, 37*(1), 167-181. https://doi.org/10.1016/0198-0149(90)90035-T

Ryan, W. B. F., S.M. Carbotte, J. Coplan, S. O'Hara, A. Melkonian, R. Arko, R.A. Weissel, V. Ferrini, A. Goodwillie, F. Nitsche, J. Bonczkowski, and R. Zemsky (2009), Global Multi-Resolution Topography (GMRT) synthesis data set, Geochem. Geophys. Geosyst., 10, Q03014, doi:10.1029/2008GC002332.

Solomon, H. (1979). A Note on the Conservation of Potential Vorticity Across a Discontinuity in Shallow Water with Application to Theories of Equatorial Dynamics and Rossby Lee Waves. *Journal of Physical Oceanography, 9*(5), 1032-1035. https://doi.org/10.1175/1520-0485(1979)009%3C1032:ANOTCO%3E2.0.CO;2

Staudigel, H., Koppers, A.A.P., Lavelle, J.W., Pitcher, T.J., & Shank, T.M. (2010). Box 1 Defining the Word "Seamount". *Oceanography, 23*(1), 20-21. https://doi.org/10.5670/oceanog.2010.85

Stern, R.J., Tamura, Y., Masuda, H., Fryer, P., Martinez, F., Ishizuka, O., & Bloomer, S.H. (2012). How the Mariana Volcanic Arc ends in the south. *Island Arc, 22*(1), 133-148. https://doi.org/10.1111/iar.12008

Strickland, J.D.H., & Parsons, T.R. (1972). A practical handbook of seawater analysis. *Fish. Res. Board Can. Bull., 167*(2), 310. http://dx.doi.org/10.25607/OBP-1791

Uitz, J., Claustre, H., Morel, A., & Hooker, S.B. (2006). Vertical distribution of phytoplankton communities in open ocean: An assessment based on surface chlorophyll. *Journal of Geophysical Research: Oceans, 111*, C8. https://doi.org/10.1029/2005JC003207

Wei, Q., Cui, Z., Wang., X., Teng., G., Qu, K., & Sun, J. (2022). Comparative Analysis of Total and Size-Fractionated Chlorophyll a in the Yellow Sea and Western Pacific. *Frontiers in Microbiology, 13*. https://doi.org/10.3389/fmicb.2022.903159

Yesson, C., Clark, M.R., Taylor, M.L., & Rogers, A.D. (2011). The global distribution of seamounts based on 30 arc seconds bathymetry data. *Deep Sea Research Part I: Oceanographic Research Papers, 58*(4), 442-453. https://doi.org/10.1016/j.dsr.2011.02.004

Zweng, M.M., Reagan, J.R., Antonov, J.I., Locarnini, R.A., Mishonov, A.V., Boyer, T.P., Garcia, H.E., Baranova, O.K., Johnson, D.R., Seidov, D., Biddle, M.M., & Levitus, S. (2013). World Ocean Atlas 2013. Volume 2, Salinity. *NOAA*. http://doi.org/10.7289/V5251G4D